Lysozyme Adsorption to Charged Surfaces. A Monte Carlo Study

Fredrik Carlsson,[†,⊥] Elin Hyltner,[†] Thomas Arnebrant,[‡] Martin Malmsten,[§] and Per Linse*,[∥]

Institute for Surface Chemistry, Box 5607, SE-114 86 Stockholm, Sweden, School of Health and Society, Malmö University, SE-205 06 Malmö, Sweden, Department of Pharmacy, Uppsala University, P.O. Box 580, SE-751 23 Uppsala, Sweden, and Physical Chemistry 1, Center for Chemistry and Chemical Engineering, Lund University, Box 124, SE-221 00 Lund, Sweden

Received: February 3, 2004; In Final Form: March 27, 2004

Lysozyme adsorption to charged surfaces was studied by Monte Carlo simulations at different protein concentrations, protein net charges, ionic strengths, and surface charge densities. The lysozyme was represented by a hard sphere with embedded positive and negative surface charges parametrically dependent on the solution pH. A short-range attractive protein−protein potential was included to represent attractive non-Coulomb forces. The charged surface was described by a hard wall with embedded charges representing a mica surface. The protein adsorption was favored by high protein concentration, high protein net charge, low ionic strength, and high surface charge density. Nevertheless, adsorption appeared also for a weakly negatively charged protein to the negatively charged surface as a result of an electrostatically favorable protein orientation at the surface. While a multipole expansion including monopole and dipole moments only was insufficient to explain preferential orientation, an expansion including also quadrupole moments provided a satisfactory picture. Finally, it was found that the short-range attraction between the proteins increased the adsorbed amount, as well as the structure in the adsorbed protein layer. The adsorbed amounts obtained compared favorably with experimental results.

Introduction

The interaction between proteins and interfaces is essential for a number of applications such as biomaterials,[1] drug delivery,[2,3] biotechnical separation methods,[4] and food technology.[5,6] The knowledge of the fundamental forces involved in protein adsorption is of great importance for understanding and controlling the interfacial behavior of proteins. Consequently, there have been considerable efforts directed to elucidate both the mechanisms of protein adsorption and the role of protein adsorption in these application areas.[7−10]

A large number of theoretical and numerical investigations of proteins interacting with surfaces have been performed.[11−22] These studies have concerned, for example, prediction of adsorption equilibria and kinetics of adsorption, examination of the electrostatic and van der Waals contributions to protein adsorption, development of equations describing adsorption isotherms for proteins and colloids, and monolayer and multilayer formation. They involved methods such as Brownian dynamics, molecular dynamics, and Monte Carlo simulations. From these investigations, it has been concluded that protein adsorption depends strongly on ionic strength and pH; thus, electrostatic interactions play a major role. For example, Oberholzer et al.[16] simulated the adsorption of latex particles and lysozyme onto uniformly charged surfaces. The colloidal particles were modeled as uniformly charged spheres. These investigators concluded that adsorption depended strongly upon the strength of the electrostatic colloid−surface attraction. For lysozyme, the adsorption was found to decrease as the ionic strength or pH increased, as a result of electrostatic screening of the protein−surface attraction and reduced protein net charge, respectively.

In the present study, the Monte Carlo simulation technique was employed to investigate a model system representing an aqueous solution of lysozyme near a mica surface. In particular, the adsorption of lysozyme and the structure of the adsorbed layer were examined. Lysozyme was chosen as the model protein because of its low adiabatic compressibility and tendency to maintain its native conformation under most conditions.[23,24] Only minor conformational changes occur on adsorption and the adsorption isotherms for native and re-adsorbed lysozyme do not differ significantly.[23,24] Another reason for choosing lysozyme was the comparatively large number of experimental data available in the literature.[8,9,24−37] Our choice of surface was governed by the high surface charge density of mica, implying that electrostatic forces are dominating, as well as by availability of some good experimental data for the well-characterized mica surface.

Our lysozyme model was constructed from X-ray crystallographic data[38] and has previously been used to examine protein self-association[39] and protein−polymer complexation[38,40] in aqueous solution. As in the study by Oberholzer et al.,[16] lysozyme is represented by a hard sphere; however, we employed a discrete charge distribution representing individual ionized amino acids. The mica surface was represented by a hard surface with embedded discrete charges. As in previous work of this type, a screened Coulomb potential was employed.

With this approach we have investigated the influence of factors such as protein concentration, protein net charge (dependent on pH), ionic strength, and surface charge density

* To whom correspondence should be addressed. E-mail: per.linse@fkem1.lu.se.
[†] Institute for Surface Chemistry.
[‡] Malmö University.
[§] Uppsala University.
[∥] Lund University.
[⊥] Present affiliation: Allied Attorneys Chemical AB, Box 24107, SE-104 51 Stockholm, Sweden.

10.1021/jp0495186 CCC: $27.50
Published on Web 06/19/2004

TABLE 1: Parameters Used in the Simulations

parameter	label	value
protein radius	R_p	18.54 Å
protein net charge	Z_p	10, 6, 0, −1, −2, −3
short-range attractive param	$\epsilon_{p,p}$	0 and 8.4×10^9 kJ/mol Å^6
surface charge spacing	d_s	6.9 and 13.8 Å
surface charge density	σ	0.021 and 0.00525 e/Å^2
temperature	T	298 K
relative permittvity	ϵ_r	78.4
ionic strength	I	0.1 and 0.2 M
box width	L_x and L_y	207 Å
box length	L_z	400 Å
number of proteins	N_p	1, 4, 16, 32, 40, 48, 64, and 128
avg protein concentration	c_{aver}	0.097−12.4 mM

on the adsorption and the structure of the adsorbed layer. Special attention was devoted to the structure of the adsorbed protein layer, including in-plane radial distribution functions and the orientation of adsorbed proteins with respect to the surface normal and neighboring proteins.

Model

Protein. Lysozyme was modeled as a hard sphere with a radius $R_p = 18.54$ Å and with each of the 32 amino acids that may be charged represented by a single site.[38] These sites were located 2 Å beneath the protein hard-sphere surface, leading to a smallest site−site separation of 4 Å, a distance reasonable for hydrated charged groups in molecular contact. A site carries either a positive charge, a negative charge, or no charge. It was assumed that an amino acid was protonated at pH < pK_a and deprotonated at pH > pK_a. In particular, pH ≈ 4.5 corresponds to a protein net charge $Z_p = 10$ with 19 positive and 9 negative charges, pH ≈ 9 to $Z_p = 6$ with 17 positive and 11 negative charges, and the isoelectric point where $Z_p = 0$ with 12 positive and 12 negative charges. In the following, the charge status of the protein is described by its net charge Z_p. Parameters characterizing the protein as well as the remaining part of the model are collected in Table 1.

Attractive non-Coulomb protein−protein interactions often play an important role, in particular, near the isoelectric point and/or at high ionic strength. These forces are of a complex nature and were as a first approximation accounted for by the attractive potential $-\epsilon_{p,p}/r_{ij}^6$, where $\epsilon_{p,p}$ (>0) is a parameter determining the strength of the non-Coulomb attraction between the proteins and r_{ij} represents the center-to-center distance between protein i and j. In an earlier work,[39] $\epsilon_{p,p}$ was adjusted to fit predicted second virial coefficients to experimental data. Moreover, $\epsilon_{p,p}$ was also set to zero to investigate the effect of the non-Coulomb attraction.

Surface. The charged mica surface was represented by a hard and smooth surface with negatively charged sites 2 Å beneath the surface. The sites were arranged in a two-dimensional quadratic lattice with a spacing $d_s = 6.9$ Å and carry the charge $Z_s = -1$ to achieve the surface charge density of a mica surface[41] $\sigma = 0.021$ e/Å^2, with e denoting the absolute value of the elementary charge. A 4-fold less charged surface, established by a 2-fold increase of d_s, was also considered to investigate the effect of the surface charge density.

Since our aim was to examine the role of the Coulomb interaction as such on the adsorption, no non-Coulomb attractive surface−protein potential was included. Moreover, this is a reasonable approximation for the highly charged mica surfaces, for which the Coulomb interaction dominates.

All systems studied contained two charged and parallel surfaces located at $z = 0$ and $z = L_z$. The separation between the surfaces L_z was selected sufficiently large to make the two protein surface layers noninteracting and to create a region of constant protein concentration (referred to as bulk) between the surface layers.

Potential Energy. All interactions were taken as pairwise additive. The total potential energy U_{tot} of the system is given as a sum of three contributions according to

$$U_{tot} = U_{hs} + U_{el} + U_{short} \tag{1}$$

The hard-sphere potential U_{hs} is given by

$$U_{hs} = \sum_{\substack{i<j \\ i,j\in p}} u_{ij}^{hs}(r_{ij}) + \sum_{i\in p} u_i^{surf}(z_i) \tag{2}$$

where the summation is over protein centers with u_{ij}^{hs} representing the hard-sphere potential between two proteins according to

$$u_{ij}^{hs}(r_{ij}) = \begin{cases} 0, & r_{ij} \geq 2R_p \\ \infty, & r_{ij} < 2R_p \end{cases} \tag{3}$$

and u_i^{surf} the hard-sphere−hard-surface potential given by

$$u_i^{surf}(z_i) = \begin{cases} 0, & R_p \leq z_i \leq L_z - R_p \\ \infty, & z_i < R_p \text{ or } z_i > L_z - R_p \end{cases} \tag{4}$$

The electrostatic potential energy U_{el} was evaluated using the screened Coulomb potential

$$U_{el} = \sum_{\substack{i<j \\ i,j\in c}} u_{ij}^{el}(r_{ij}) = \sum_{\substack{i<j \\ i,j\in c}} \frac{Z_i Z_j e^2}{4\pi\epsilon_0\epsilon_r} \frac{1}{r_{ij}} \exp(-\kappa r_{ij}) \tag{5}$$

where the summation extends over protein sites and surface charges with ϵ_0 denoting the permittivity of vacuum, ϵ_r the relative permittivity of the solvent, Z_i the charge of the site i, and κ the inverse Debye screening length. The non-Coulomb attractive potential U_{short} is given by

$$U_{short} = -\sum_{\substack{i<j \\ i,j\in p}} \frac{\epsilon_{p,p}}{r_{ij}^6} \tag{6}$$

where the summation extends over protein centers with $\epsilon_{p,p}$ being the parameter determining the strength of the non-Coulomb attraction.

The Debye screening length κ^{-1} entered in eq 5 is given by $\kappa^{-1} = [\{e^2\}/\{(\epsilon_0\epsilon_r k_B T)\} \sum_m Z_m^2 c_m]^{-1/2}$, where k_B is Boltzmann's constant, T the temperature, Z_m the valence, and c_m the bulk concentration of salt species m. In this study, the salt concentration is referred to as ionic strength $I = (1/2)\Sigma_m Z_m^2 c_m$. Throughout, $T = 298$ K and $\epsilon_r = 78.4$, representing water, have been used. Under these conditions, the relation between κ^{-1} and I is simplified to $\kappa^{-1}/\text{Å} = 3.04/(I/\text{M})^{0.5}$.

Systems. Several systems at different conditions were examined. A reference system, characterized by an ionic strength $I = 0.1$ M and a surface charge density $\sigma = 0.021$ e/Å^2, the latter corresponding to mica, was investigated at protein net charges $Z_p = 10$, 6, 0, −1, −2, and −3. Simulations were performed from $N_p = 1$ to 128 proteins, corresponding to average protein concentrations $c_{aver} = 0.097-12.4$ mM. Departing from the reference system with $Z_p = 6$, three other systems were considered. In system 1, the short-range attraction between proteins is removed, that is, $\epsilon_{p,p} = 0$; in system 2, the ionic strength is increased to $I = 0.2$ M; and in system 3, the surface

TABLE 2: Overview of the Systems Investigated

system	σ (e/Å^2)	I (M)	$\epsilon_{p,p}$ (kJ/mol Å^6)	Z_p
reference	0.021	0.1	8.4×10^9	10, 6, 0, −1, −2, −3
1	0.021	0.1	0	6
2	0.021	0.2	8.4×10^9	6
3	0.00525	0.1	8.4×10^9	6

TABLE 3: Corresponding Net Charge, Magnitude of Dipole Vector, Diagonal Components of the Diagonalized Irreducible Quadrupole Tensor, and the Angles between the Directions of the Dipole Moments and the Diagonal Components of the Quadrupole Tensor of the Lysozyme Model

Z_p	m (e Å)	Q_{11} (e Å^2)	Q_{22} (e Å^2)	Q_{33} (e Å^2)	γ_{m1} (deg)	γ_{m2} (deg)	γ_{m3} (deg)
10	24.2	347.7	−1017.1	669.4	74.7	55.1	39.0
6	21.5	−75.0	−706.1	781.9	83.4	63.4	27.6
0	28.8	103.8	−500.0	396.2	62.3	61.8	41.5
−1	44.1	−534.5	29.0	505.5	43.3	59.9	62.1
−2	43.8	129.3	−709.4	580.0	41.1	76.1	52.2

charge density is 4-fold reduced to $\sigma = 0.00525$ e/Å^2. See also Table 2. Simulations with $I = 0.3$ M were also performed; however, no adsorption took place so data for this condition will not be given.

Charge Multipole Expansion. A representation of the charge distribution of lysozyme in terms of the three first multipole moments will play a central role in our analysis of the orientation of lysozyme near the charged surfaces. These moments are the net charge Q, the dipole vector $\mathbf{m}$, and the irreducible quadrupole tensor $\mathbf{Q}$, given by

$$Q = eZ_p = e\sum_i Z_i \tag{7}$$

$$\mathbf{m} = e\sum_i Z_i \mathbf{r}_i \tag{8}$$

$$\mathbf{Q} = \frac{1}{2} e\sum_i Z_i (3\mathbf{r}_i\mathbf{r}_i - r_i^2\mathbf{E}) \tag{9}$$

where $\mathbf{r}_i$ is the position of site i relative to the protein center and $\mathbf{E}$ the unit matrix. Of special concern are the following: (i) the magnitude m and the direction $\mathbf{n}_m$ of the dipole vector [$\mathbf{m} = m\mathbf{n}_m$] and (ii) the magnitudes $Q_{\alpha\alpha}$ and the directions $\mathbf{n}_\alpha$, $\alpha = 1, 2, 3$, of the diagonal components of the diagonalized irreducible quadrupole tensor $\mathbf{Q}$ [$Q_{\alpha\alpha}$ are the eigenvalues and $\mathbf{n}_\alpha$, $\alpha = 1, 2, 3$, the eigenvectors of $\mathbf{Q}$ according to $\mathbf{X}^{-1}\mathbf{Q}\mathbf{X} = \mathrm{diag}(Q_{11}, Q_{22}, Q_{33})$ with $\mathbf{X} = (\mathbf{n}_1^T, \mathbf{n}_2^T, \mathbf{n}_3^T)$].

Table 3 provides a summary of m and $Q_{\alpha\alpha}$, $\alpha = 1, 2, 3$, at different Z_p. Of value are also the angles $\gamma_{m\alpha}'$ between $\mathbf{n}_m$ and $\mathbf{n}_\alpha$, $\alpha = 1, 2, 3$. By symmetry, $\mathbf{n}_\alpha$, $\alpha = 1, 2, 3$, is arbitrary by the factor −1. In the following, $\gamma_{m\alpha}$ will refer to the smallest angle of $\gamma_{m\alpha}'$ and $\pi - \gamma_{m\alpha}'$ and Table 3 also provides a summary of $\gamma_{m\alpha}$, $\alpha = 1, 2, 3$. The location of the charged sites and the directions $\mathbf{n}_m$ and $\mathbf{n}_\alpha$, $\alpha = 1, 2, 3$, in the protein coordinate frame $x'y'z'$ at different Z_p are graphically shown in Figure 1.

Method

The model systems were solved by Metropolis Monte Carlo (MC) simulations[42] in the canonical ensemble, that is, at a constant number of particles, volume, and temperature. The simulated systems contained the proteins enclosed in a rectangular box with box lengths $L_x = L_y = 207$ Å and $L_z = 400$ Å. The two charged and hard surfaces were placed at $z = 0$ and $z = L_z$, and periodic boundary conditions were applied in the x-

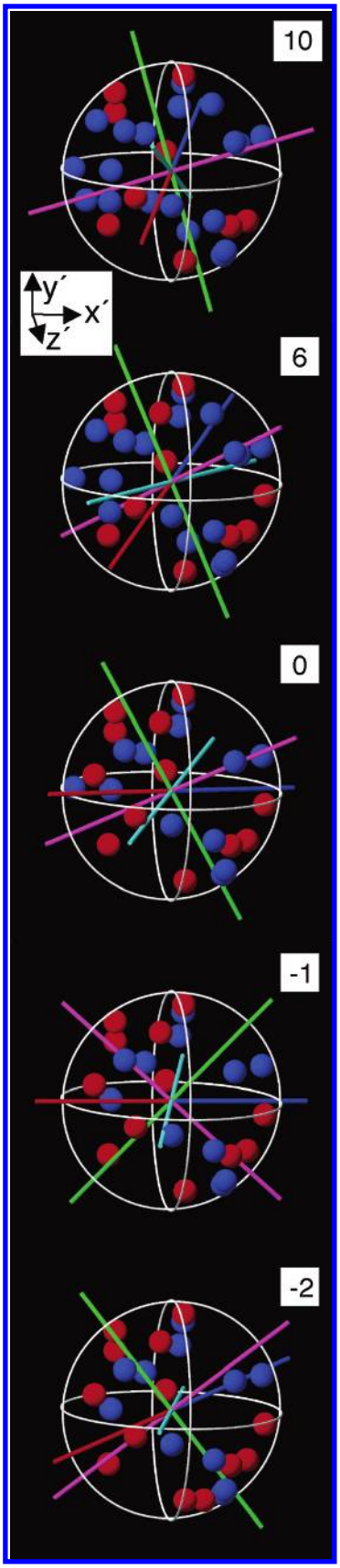

Figure 1. Illustration of the lysozyme model at $Z_p = 10, 6, 0, -1$, and −2 (top to bottom), displaying the hard-sphere radii, the location of the positively (blue spheres) and negatively (red spheres) charged sites, the direction of the dipole vector $\mathbf{n}_m$ (positive ends in blue and negative ends in red), the direction of the diagonal components of the diagonalized irreducible quadrupole tensor $\mathbf{n}_\alpha$ ($\mathbf{n}_1$ in pink, $\mathbf{n}_2$ in green, and $\mathbf{n}_3$ in magenta), and the protein coordinate frame $x'y'z'$.

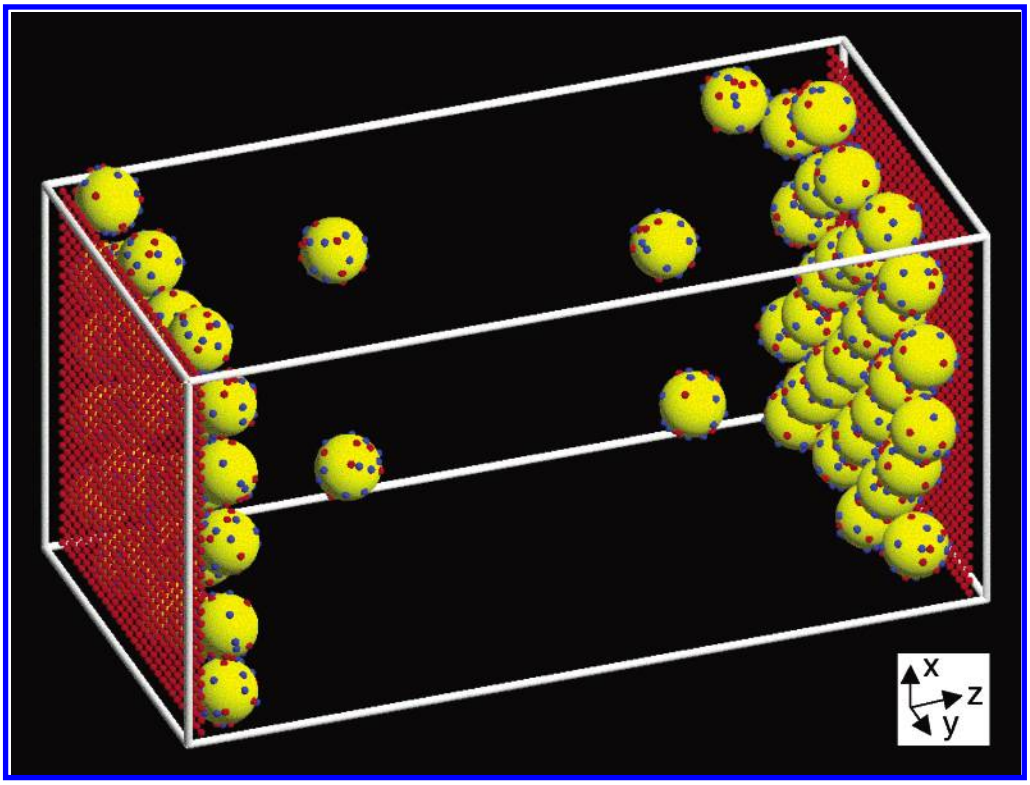

Figure 2. Illustration of the simulation box including the external coordinate frame *xyz* and a typical configuration taken from the end of the simulation of the reference system at $Z_p = 6$ with $c_{aver} = 6.4$ mM, showing the surface charges (red dots, left and right edges of the box) and the $N_p = 64$ proteins (yellow spheres) with positively (blue dots) and negatively (red dots) charged sites. The hard spheres of the proteins are reduced by 2 Å to 16.54 Å to enable visualization of the charged sites.

and *y*-directions. All interactions were truncated using a spherical cutoff $R_{cut} = 100$ Å, leading to $u_{ij}^{el}(r_{ij} = R_{cut})/k_BT < 2 \times 10^{-6}$. Surface-related properties were taken as an average over the two independent surfaces.

Translational displacements in the *x*-, *y*-, and *z*-directions and rotational displacements of the protein around a randomly selected axis constituted the trial moves in the simulations. The translational displacements were uniformly sampled in the interval $[-\Delta_p/2, \Delta_p/2]$ and the angular displacements in the interval $[-\theta_p/2, \theta_p/2]$ with $\Delta_p = 10$ Å and $\theta_p = 360°$ being used.

Since the simulations were performed at a constant number of proteins and at constant volume, the average protein concentration c_{aver} is fixed. At strong adsorption conditions with small N_p, the bulk concentration c_{bulk} becomes smaller than c_{aver}. Since the bulk concentration, or rather the chemical potential, governs the adsorption, the bulk concentration obtained will be employed when discussing adsorption isotherms. The structure of the adsorbed protein layers will to a large extent be examined at similar adsorbed amounts. Proteins within the distance $R_p + \delta$ from a surface with $\delta = 5$ Å were defined to be adsorbed to that surface.

Equilibrium simulations were carried out using at least 10^4 MC passes (trial moves per protein) followed by production simulations involving at least 10^6 MC passes. The mobility in the configurational space was examined by considering the mean residence "time" τ of a protein being adsorbed. It was determined by integrating the normalized residence "time" correlation function $\psi(n_{pass})$, denoting the probability that a protein was still adsorbed at a surface after n_{pass} MC passes given that it was initially adsorbed at that surface. For the reference system at $Z_p = 10$ and 6, the adsorption is very strong and $\tau \approx 10^6$ passes was obtained, but otherwise at weaker adsorption $\tau \approx 10^3-10^4$ passes. In the former case, therefore, only a few exchanges of proteins between the surface layer and bulk occurred, but nevertheless the simulations were sufficiently extended to give an accurate description of the structure of the adsorbed layers.

All simulations were carried out using the integrated Monte Carlo/molecular dynamics/Brownian dynamics simulation package MOLSIM.[43]

Results

The simulation box and a typical configuration of the reference system at $Z_p = 6$ with $N_p = 64$, giving $c_{aver} = 6.2$ mM and $c_{bulk} = 0.89$ mM, are shown in Figure 2. At this condition, a strong attraction between the protein and the charged surface is present. Nearly all proteins are adsorbed to the surfaces, which to a large degree are covered by the proteins.

In the following, the protein adsorption will be examined in terms of adsorption isotherms and the orientation of the proteins with respect to the surface normal. Thereafter, the lateral structure of proteins near the surface and the orientation of proteins relative to each other will be considered.

Adsorption Isotherms. The adsorbed amount of lysozyme at different conditions is shown in Figure 3. The adsorbed amount was converted to mg/m^2 by using the molecular weight 14320 g/mol of lysozyme.[44]

Figure 3a shows the adsorbed amount Γ as a function of bulk protein concentration for the reference system at the protein net charges $Z_p = 10$, 6, 0, -1, and -2. At the two highest net charges, adsorption appears already at sub-micromolar protein concentration. The isotherms display an increasing adsorbed amount as the protein concentration is increased, followed by saturation at higher bulk protein concentration. In the log-lin representation used, sigmoidal isotherms are obtained. At saturation ($c_{bulk} \approx 10$ mM), the absorption amounts to $\Gamma = 1.65$ mg/m^2, corresponding to a surface coverage of projected

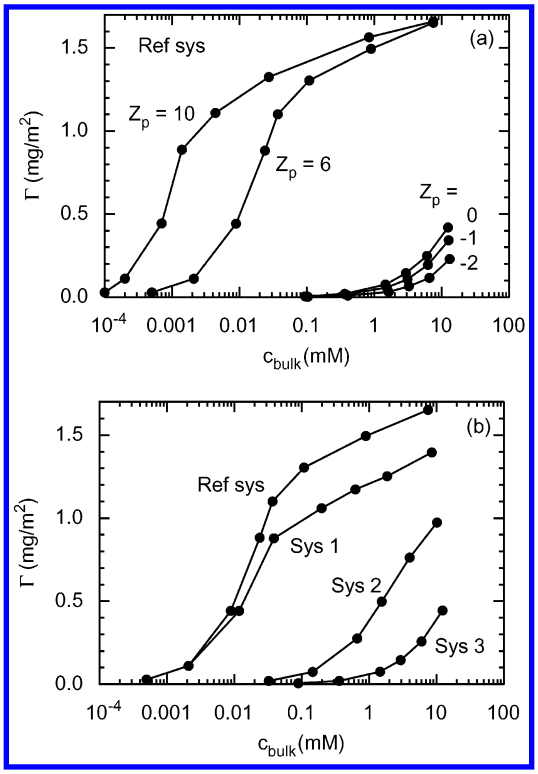

Figure 3. Adsorbed amount of protein Γ as a function of bulk protein concentration c_{bulk} for (a) the reference system at indicated protein net charge Z_p and (b) for indicated systems at the protein net charge $Z_p = 6$. Proteins with their centers within 5 Å from a surface were considered as being adsorbed. The statistical uncertainty of the adsorbed amount ranges from ≤0.5% at high Γ to ≤4% at small Γ.

spheres of $\eta = 0.76$. For comparison, a cubic or hexagonal close-packed layer of hard disks corresponds to a surface coverage of $\eta = \pi/4 \approx 0.79$ or $\pi/(2\sqrt{3}) \approx 0.91$, respectively. The adsorbed layer at saturation is therefore dense (cf. the packing at $\Gamma = 1.50$ mg/m^2 given in Figure 2).

Adsorption isotherms near the isoelectric point were also examined. At zero net charge ($Z_p = 0$), still a significant adsorption appears which starts at a millimolar protein concentration. Also for the cases at which the surface and the protein have net charges of the *same* sign ($Z_p = -1$ and -2) protein adsorption appears. We anticipate a preferential orientation of the proteins near the surface, where the positive charges are nearer and the negative charges further away from the surface to still establish a net attractive electrostatic interaction. Obviously, a nonspherical protein charge distribution is a prerequisite for the observed adsorption at $Z_p < 0$. However, we observed that at $Z_p = -3$ the proteins are depleted from the charged surfaces, and thus with this net charge an effective electrostatic protein−surface repulsion prevails.

The adsorption isotherms for the reference system at $Z_p = 6$ and for systems 1−3 are provided in Figure 3b. In the case of no short-range attractive protein−protein attraction (system 1), the onset of the adsorption is as expected unaffected, but at higher bulk protein concentration the rise of the adsorption isotherm is slower. Hence, the short-range protein attraction facilitates adsorption when the adsorbed amount is substantial, a reasonable effect since making the protein−protein interaction less repulsive by adding the short-range attraction to the repulsive electrostatic interaction at fixed protein−surface interaction should favor the adsorbed state where the local protein density is larger. Furthermore, the increase of the ionic strength from $I = 0.1$ M to $I = 0.2$ M (system 2) or the 4-fold reduction of the surface charge density (system 3) results in shifts of the adsorption isotherms to a 100-fold and a 1000-fold, respectively, higher bulk protein concentration. The decreased adsorption at higher ionic strength is driven by the larger screening of the electrostatic interactions, making the protein−surface attraction weaker. Analogously, a reduced surface charge density leads to a weakening of the electrostatic protein−surface attraction through a smaller electrical field originating from the charged surface.

To conclude, the adsorption is increased by (i) increasing bulk concentration, (ii) increasing protein charge (by reducing pH), (iii) increasing short-range protein−protein attraction, (iv) decreasing salt concentration, and (v) increasing surface charge density. Noticeably, adsorption due to electrostatic interactions may also appear with proteins of the *same* net charge as the charged surface.

Normal Protein Distribution. The protein distribution perpendicular to the surface is displayed in Figure 4 using the distribution function $c(z)/c_{aver}$, which expresses the relative concentration of a protein at a distance z from the surface as compared to the average concentration. At distances $z < R_p$, $c(z)/c_{aver}$ is zero because of the hard-sphere−hard-surface repulsion. Far from the surface, $c(z)/c_{aver} < 1$ since typically $c_{bulk} < c_{aver}$ (as discussed in the Method section).

Figure 4a shows $c(z)/c_{aver}$ for the reference system at $Z_p = 6$ at three different numbers of proteins ($N_p = 1$, 16, and 128), corresponding to the first, an intermediate ($\Gamma \approx 0.5$ mg/m^2), and the last point of the adsorption isotherm given in Figure 3a. The function $c(z)/c_{aver}$ displays a sharp peak at protein−surface contact, and the most uneven distribution ($c(R_p)/c_{aver} \approx 280$) appears for the two cases with the smallest amount of protein. For the largest amount of protein, a local maximum appears at $z \approx 55$ Å, indicating the appearance of a second protein layer. However, the height of this second peak is 70-fold smaller than that of the first one, indicating merely individual proteins added to the primary adsorbed layer. The height of the second peak is reduced to 1.2 (data not shown) when the short-range protein−protein attraction is removed, showing that the short-range attraction is important for the formation of the second layer.

The transversal protein distributions for the reference system at different protein net charges, but at similar adsorbed amounts ($\Gamma \approx 0.5$ mg/m^2), are shown in Figure 4b. It is seen that the thickness of the adsorbed layer is similar at $Z_p = 6$ and 10 and much larger at $Z_p = 0$. Hence, at conditions of equal amount of adsorbed proteins, the adsorbed layer becomes thinner as the protein net charge increases, an effect of the stronger electrostatic protein−surface attraction.

The corresponding distribution functions for the reference system and systems 1, 2, and 3 at $Z_p = 6$ and $\Gamma \approx 0.5$ mg/m^2 are displayed in Figure 4c. A comparison of data for the reference system and system 1 shows that the short-range protein attraction has no influence on the transversal protein distribution at this Γ. However, a weaker protein−surface interaction, by increasing the salt concentration or by reducing the surface charge density, leads to a broadening of the adsorbed layer, again compared at equal adsorbed amounts. For systems 2 and 3, as well as for the reference system at $Z_p = 0$, a weak second maximum appears at $z \approx 55$ Å.

Hence, for strong adsorption the adsorbed protein layer is thin, extending to $z = R_p + \delta$ with $\delta \approx 5$ Å, which motivates our criterion for evaluating the adsorbed amount used above. For a similar amount of adsorbed proteins, the thickness of the adsorbed layer decreases as the protein−surface interaction is

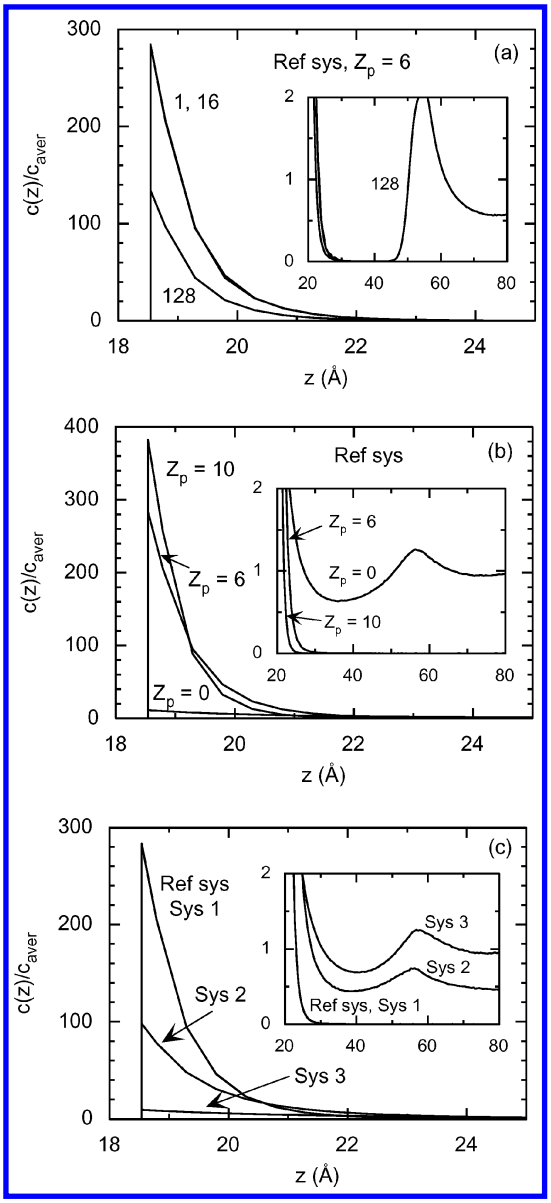

Figure 4. Normal protein distribution function $c(z)/c_{aver}$ for (a) the reference system at the protein net charge $Z_p = 6$ and indicated number of proteins N_p, (b) the reference system at indicated protein net charge Z_p and $\Gamma \approx 0.5$ mg/m^2 ($N_p = 16$, 16, and 128 at $Z_p = 10$, 6, and 0, respectively), and (c) the indicated systems at the protein net charge $Z_p = 6$ and $\Gamma \approx 0.5$ mg/m^2 ($N_p = 16$, 32, and 128 for the reference system, system 2, and system 3, respectively). The inserts show a magnification of $c(z)/c_{aver}$ for the distances $z = 20-80$ Å. In (c), the curves for the reference system and system 1 are indistinguishable.

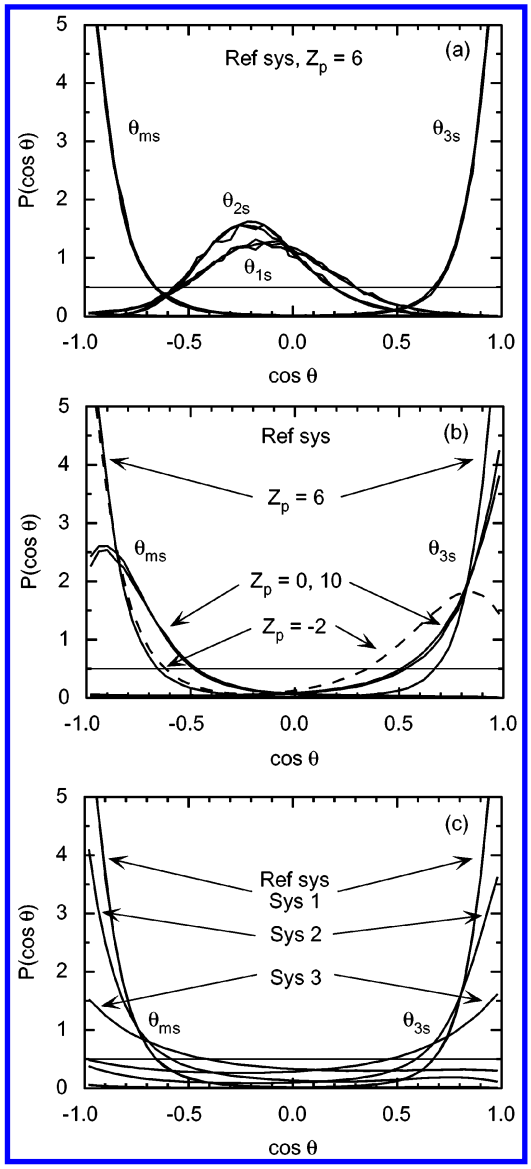

Figure 5. Normalized orientational distribution functions $P(\cos \theta_{ms})$ and $P(\cos \theta_{\alpha s})$, $\alpha = 1, 2, 3$, of adsorbed proteins for (a) the reference system at the protein net charge $Z_p = 6$ and $N_p = 1$, 16, 128, (b) the reference system at indicated protein net charge Z_p and $\Gamma \approx 0.5$ mg/m^2, and (c) the indicated systems at the protein net charge at $Z_p = 6$ and $\Gamma \approx 0.5$ mg/m^2. The thin solid lines at 0.5 denote P for isotropic orientations. In (a), the curves for different N_p are similar; in (b), the curves at $Z_p = 0$ and 10 are similar and the curve at $Z_p = -2$ is dashed; and in (c), the curves for the reference system and system 1 are indistinguishable. For clarity, in (b) and (c) only $P(\cos \theta_{ms})$ and $P(\cos \theta_{1s})$ are given.

increased, either by (i) increasing protein charge, (ii) decreasing salt concentration, or (iii) increasing surface charge density.

Protein Orientation. The orientation of adsorbed proteins relative to the surface normal will now be examined. Two types of properties are employed, that is, probability distribution functions $P(\cos \theta)$, where θ is an angle between a protein axis and the positive surface normal, and contour diagrams displaying protein orientation probabilities. Again proteins located within the distance $R_p + \delta$ from a surface with $\delta = 5$ Å are selected.

Probability Distribution Functions. Consider (i) the angle θ_{ms} between the direction of the dipole vector $\mathbf{n}_m$ and the positive surface normal $\mathbf{n}_s$ and (ii) the angles $\theta_{\alpha s}$, $\alpha = 1, 2, 3$, between the directions of the diagonal components of the diagonalized irreducible quadrupole tensor $\mathbf{n}_\alpha$, $\alpha = 1, 2, 3$, and the positive surface normal $\mathbf{n}_s$. Figure 5 displays the four normalized probability distributions $P(\cos \theta_{ms})$ and $P(\cos \theta_{\alpha s})$, $\alpha = 1, 2, 3$, at various conditions. The sign ambiguity of $\mathbf{n}_\alpha$ leads to a sign ambiguity of $\cos \theta_{\alpha s}$, $\alpha = 1, 2, 3$, implying that the preferential orientation of $Q_{\alpha\alpha}$ equally well could have been described by $P(-\cos \theta_{\alpha s})$

The four distribution functions for the reference system at $Z_p = 6$ and different adsorbed amounts are given in Figure 5a. Since the different distribution functions from a single adsorbed protein to a saturated layer of adsorbed proteins essentially superimpose each other, we directly conclude that the orientation of the adsorbed proteins with respect to the surface normal is *independent* of the adsorbed amount. Hence, at these conditions the protein−surface interaction is much more important than

the protein−protein interaction for the orientation of the proteins relative to the surface normal.

In more detail, $P(\cos\theta_{ms})$ peaks at $\cos\theta_{ms} = -1$ and is essentially zero for $\cos\theta_{ms} > -0.4$, indicating a strong preferential orientation of the dipole moment with respect to the surface normal, with the positively charged end of the dipole vector closer to the negatively charged surface. Moreover, $P(\cos\theta_{3s})$ is equally askew, showing that the preferential orientation of the direction of the quadruple component Q_{33} is equally strong. Table 3 shows that the value of Q_{33} is positive and large, and hence the strong preferential orientation of $\mathbf{n}_3$ is coupled with an advantageous electrostatic interaction between the quadruple component Q_{33} and the negatively charged surface. In addition, an inspection of Figure 1 and Table 3 shows that the angle between $\mathbf{n}_m$ and $\mathbf{n}_3$ is fairly small (28°). Hence, the strong preferential orientation of $\mathbf{m}$ and Q_{33} is by necessity linked and therefore also synergistic. The preferential orientations of the remaining two quadrupole components display a maximum at $\theta_{\alpha s} \approx -0.2$, showing that they are preferentially orientated essentially parallel to the surface. Table 3 shows that Q_{11} is close to zero and nearly perpendicular to $\mathbf{n}_m$, whereas Q_{22} has a considerable negative magnitude and its direction forms a 63° angle with $\mathbf{n}_m$. The distribution of the more negative one, Q_{22}, is somewhat more peaked.

Two of the four distribution functions for the reference system at different protein net charges and similar adsorbed amounts ($\Gamma \approx 0.5$ mg/m^2) are shown in Figure 5b. Generally, the overall appearance of the distribution functions is similar at different Z_p. Nevertheless, two important observations are recognized among $Z_p = 0$, 6, and 10: (A) the distributions $P(\cos\theta_{ms})$ and $P(\cos\theta_{3s})$ at $Z_p = 0$ and 10 are *less* askew as compared to $Z_p = 6$ and (B) at $Z_p = 0$ and 10 the maximum in $P(\cos\theta_{ms})$ appears at $\cos\theta_{ms} \approx -0.9 > -1$, whereas the maximum in $P(\cos\theta_{3s})$ still appears at $\cos\theta_{3s} = 1$. We connect observation (A) with the fact that the angle γ_{m3} between $\mathbf{n}_m$ and $\mathbf{n}_3$ is larger for $Z_p = 0$ and 10 than at $Z_p = 6$ (see Table 3); hence, the larger γ_{m3} weakens the cooperativity between $\mathbf{m}$ and Q_{33} to establish a common preferred direction relative to the surface normal. From observation (B), we infer that the quadrupole moment−surface interaction is *stronger* than the dipole moment−surface interaction.

It was previously found that also net negatively charged proteins are able to adsorb to the negatively charged surface (Figure 3a). Figure 5b (dashed curves) shows that the preferential orientation at this condition is of equal strength. Interestingly, $P(\cos\theta_{ms})$ peaks at $\cos\theta_{ms} = -1$, whereas $P(\cos\theta_{3s})$ has its maximum at $\cos\theta_{3s} = 0.8 < 1.0$. The weakened cooperativity is attributed to the large angle $\gamma_{m3} = 52°$. The observation that now the dipole moment m is of larger importance than the quadrupole moment Q_{33} for the most preferred orientation, most likely originates from m being up to twice as large as compared with the case $Z_p \geq 0$ (see Table 3).

Finally, Figure 5c shows the distributions for the reference system and for systems 1, 2, and 3, again at similar amounts of adsorbed proteins. The distribution functions for system 1 are in practice identical to those of the reference system; hence, the short-range protein attraction does not influence the orientation of the proteins at the present conditions. The distribution functions are systematically less peaked for system 2 with the 2-fold higher salt concentration, demonstrating a weaker preferential orientation. Furthermore, the 4-fold reduction of the surface charge density leads to an even stronger reduction of the preferential orientation. We notice that the weaker protein−surface attraction in system 3 as compared to that in system 2 is manifested by (i) an adsorption isotherm shifted to higher bulk concentration (Figure 3b) and (ii) a thicker adsorbed layer (Figure 4c) of less preferentially oriented proteins (Figure 5c).

Contour Diagrams. A complementary picture of the preferential orientation of the proteins in the adsorbed layer is provided by considering the probability of the point $\mathbf{r}' \equiv (x', y', z')$ on the protein hard-sphere surface to be *closest to* the charged surface. Since the magnitude of $\mathbf{r}'$ is the same for all points, the point will be represented by its polar angles θ and ϕ, conventionally defined according to $x' = r' \sin\theta \cos\phi$, $y' = r'\sin\theta \sin\phi$, and $z' = r'\cos\theta$. This characterization of the protein orientation is represented by a two-dimensional probability distribution $P(\cos\theta, \phi)$, where $\cos\theta$ ranges from −1 to 1 and ϕ from 0 to 360°. Figure 6 shows five such probability distributions as contour diagrams for some selected conditions. In the diagrams, the location of the directions $\mathbf{n}_m$ (labeled with "+" and "−" signs) and $\mathbf{n}_\alpha$, $\alpha = 1, 2, 3$, (labeled "1", "2", and "3"; cf. directions in Figure 1), are also included, which will be essential for the discussion. See also the caption of Figure 6 for further details.

Figure 6a−c displays the contour diagrams for the reference system at different protein net charges and similar adsorbed amounts ($\Gamma \approx 0.5$ mg/m^2). Starting with $Z_p = 6$ (Figure 6b), a prominent probability maximum of $P = 0.031$ appears at $(\cos\theta, \phi) = (-0.68, 15°)$ and the location of this maximum is very close to the direction of the positive end of the dipole vector m (labeled "+") and the direction of Q_{33} (labeled "3"). Since the equi-probability lines are approximately logarithmically separated, the fluctuations about the most preferred directions are small, as already anticipated from Figure 5a. The fluctuations from the most preferred direction are not isotropic. Instead, a ridge of enhanced probability from $\mathbf{n}_3$ to $\mathbf{n}_1$ is present, demonstrating that fluctuations bringing $\mathbf{n}_1$ toward the charged surface (reducing θ_{2s}) are more frequent than fluctuations bringing $\mathbf{n}_2$ toward the surface. Considering that $Q_{11} = -75\ e$ Å^2 and $Q_{22} = -706\ e$ Å^2, the more negative Q_{22} should more strongly restrict the $\mathbf{n}_2$ axis from coming close to the negatively charged surface. The corresponding contour diagram at $\Gamma \approx 1.65$ mg/m^2 (data not shown) is virtually identical to that at $\Gamma \approx 0.5$ mg/m^2, confirming the notion that the orientation at these conditions is not dependent on the adsorbed amount.

Figure 6a displays the contour diagram at $Z_p = 10$. The overall picture resembles that for the lower net charge $Z_p = 10$. However, (i) the most likely point (−0.82, 355°) has a smaller probability, $P = 0.018$, (ii) the region in the $(\cos\theta, \phi)$ space with high probability is more extended, and (iii) the positive end of the dipole axis $\mathbf{n}_m$ is substantially displaced from this region, all observations being in accord with conclusions made from Figure 5b. Second, the ridge toward larger $\cos\theta$ is more extended and also the opposite orientation ≈(−0.5, 190°) possesses an enhanced probability. The latter effects arise from quadrupole moment $Q_{11} = 348\ e$ Å^2 being positive and hence interacting favorably with the negatively charged surface. Some features of the contour diagram at $Z_p = 0$ given in Figure 6c are similar to those at $Z_p = 10$, in particular, the displacement of the positive end of $\mathbf{n}_m$ from the region with largest probability and the ridge toward larger $\cos\theta$, whereas other features, such as the location and the high probability of the most likely point, is closer to those of $Z_p = 6$.

Contour diagrams for the reference system with net negatively charged proteins have also been examined (data not shown). These confirm that the orientational distribution is similar to that at $Z_p = 0$. At $Z_p = -2$, the maximal probability $P = 0.027$

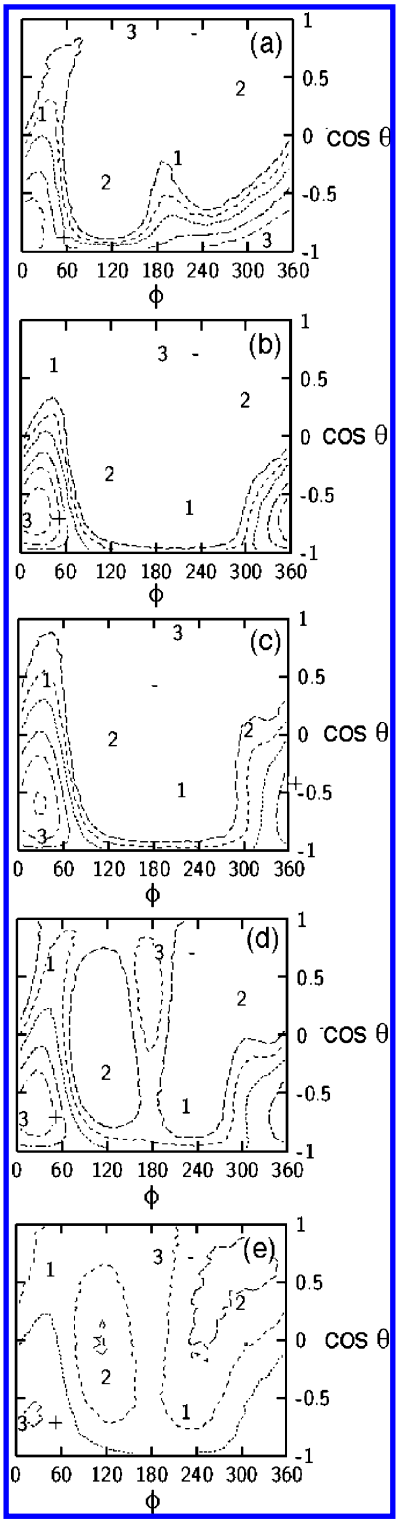

Figure 6. Normalized two-dimensional probability distributions $P(\cos\theta, \phi)$ of adsorbed proteins expressing the probability of a point on the protein surface, characterized by the polar angles θ, ϕ in the protein coordinate frame (as defined in, e.g., Figure 1), to be closest to the charged surface for the reference system at (a) $Z_p = 10$ and $N_p = 16$, (b) $Z_p = 6$ and $N_p = 16$, and (c) $Z_p = 0$ and $N_p = 128$, as well as (d) system 2 and (e) system 3, conditions corresponding to $\Gamma \approx 0.5$ mg/m^2. The largest probabilities are (a) 0.018, (b) 0.031, (c) 0.022, (d) 0.018, and (e) 0.0052, and the contour lines are given at $P = 0.02$, 0.01, 0.005, 0.002, 0.001, and 0.0005 (when applicable). For an isotropic distribution, $P = 0.0014$. Left and right ordinates represent identical orientations, whereas the top and bottom abscissas denote two different points (the poles of the spherical polar coordinate system). The location of the directions $\mathbf{n}_m$ (labeled "+" and "−") and $\mathbf{n}_\alpha$, $\alpha = 1, 2, 3$, (labeled "1", "2", and "3") are also given.

appears at (−0.575, 35°), very close to the location of the positive end of the dipole vector (cf. discussion of Figure 5b).

The contour diagrams at higher salt concentration (system 2) and lower surface charge density (system 3), both at $\Gamma \approx 0.5$ mg/m^2, are displayed in parts (d) and (e), respectively, of Figure 6. Although the most probable orientations remain similar, their probabilities have reduced to $P = 0.018$ and 0.0052, respectively, and the probabilities of reverse orientations are strongly increased. Regarding system 2, a second maximum involving a reversal of the orientation with respect to the $\mathbf{n}_3$ axis ($\cos\theta \rightarrow -\cos\theta$ and $\phi \rightarrow \phi + 180°$) appears, and two global minima related to the negative quadrupole moment Q_{22} are present. In the case of system 3, the contour diagram is even smoother. The second maximum is less prominent (not visible with the present selection of contour lines) and the two minima are well-developed; again, these features are related to the quadrupole moments.

In brief, the analysis of the orientation of adsorbed proteins demonstrates that the proteins in general have prominent preferred relative orientations with respect to the surface normal. The strength of the preferred orientation is not necessarily coupled to a strong adsorption. The case of the reference system with the net negative charge $Z_p = -2$ is an example of weak adsorption still characterized by a strong preferential orientation. However, in the cases when the electrostatic interaction is more screened or the surface charge density reduced, also leading to a weaker adsorption, the preference for specific orientations is reduced. Furthermore, our analysis demonstrates that the preferential orientation cannot satisfactorily be explained by the dipole moment only, but it seems that it is sufficient to include the next multipole moment, that is, the quadrupole, to explain all main features of the preferential orientations observed.

Lateral Protein Distribution. The lateral (in-plane) structure of the protein surface layer was determined by employing two-dimensional radial distribution functions (rdf's) $g_{lat}(\rho)$ with $\rho = (x^2 + y^2)^{1/2}$. The lateral rdf's were evaluated using the x- and y-coordinates of proteins adsorbed to the surfaces, disregarding their dispersion in the z-direction. The protein−protein separation in the z-direction is small (at most 5 Å) as compared to the protein diameter (37 Å), making such projection useful. Figure 7 shows the lateral rdf's for some selected conditions. As for three-dimensional rdf's, the two-dimensional analogue is zero at short distances, where hard-sphere repulsion appears and approaches unity at large separations where spatial correlations have vanished.

Figure 7a displays $g_{lat}(\rho)$ for the reference system at $Z_p = 6$ with a different number of proteins (solid curves). At $N_p = 16$, corresponding to $\Gamma \approx 0.5$ mg/m^2, a considerable maximum appears at $r \approx 2R_p$ and very little structure beyond the first maximum is found. At $N_p = 128$, corresponding to the highest adsorbed amount $\Gamma \approx 1.65$ mg/m^2 and a surface coverage $\eta = 0.76$, a much more prominent in-plane structure is obtained. The height of the maximum at contact is higher, a second shell of neighboring proteins with a split peak appears, and $g_{lat}(\rho)$ becomes nearly zero in the intervening minimum, consistent with the dense structure of the adsorbed layers shown in Figure 2.

The lateral rdf's of a two-dimensional hard-disk system at otherwise identical conditions (filled circles) are also shown in Figure 7a. The discrepancy between $g_{lat}(\rho)$ and the two-dimensional hard-disk rdf at the lower adsorbed amount shows that the short-range protein attraction leads to a considerable increased probability of protein contacts in the adsorbed layer, that is, a clustering of adsorbed proteins. However, the similarity

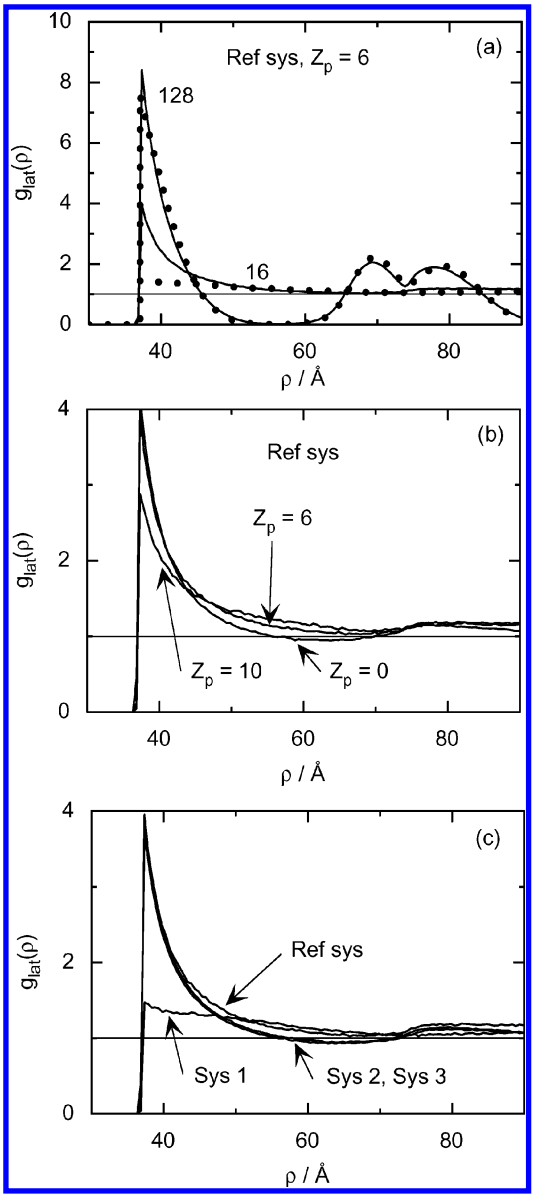

Figure 7. Lateral protein radial distribution function $g_{lat}(\rho)$ of adsorbed proteins for (a) the reference system at the protein net charge $Z_p = 6$ and indicated number of proteins N_p, (b) the reference system at indicated protein net charge Z_p and $\Gamma \approx 0.5$ mg/m^2, and (c) the indicated systems at the protein net charge at $Z_p = 6$ and $\Gamma \approx 0.5$ mg/m^2 (solid curves). The thin solid lines refer to homogeneous distributions. In (c), the curves for systems 2 and 3 are essentially indistinguishable. In (a), the corresponding $g_{2D}(\rho)$ for a two-dimensional hard-disk system at otherwise identical conditions as for the reference system for the two values of N_p are also given (filled circles).

of the corresponding rdf, including the split of the second peak, at $\Gamma \approx 1.65$ mg/m^2 implies that at a high adsorbed amount the lateral packing is nearly exclusively controlled by packing effects. The split of the second peak is a signature of a glassy state, which appears at $\eta > 0.71$.[45]

The lateral structures for the reference system at different net charges and $\Gamma \approx 0.5$ mg/m^2 are shown in Figure 7b. To the first order, the lateral rdf's are similar. However, the stronger electrostatic protein−protein repulsion at $Z_p = 10$ gives rise to a less prominent first maximum, and at $Z_p = 0$ a weak minimum at $\rho \approx 65$ Å appears.

Finally, the corresponding rdf's for the reference system and systems 1, 2, and 3 at similar adsorbed amounts are given in Figure 7c. As seen, the omission of the short-range attraction (system 1) leads to a much less prominent first maximum. In fact, the lateral rdf for system 1 virtually agrees with that for the corresponding two-dimensional hard-disk system at otherwise identical conditions (cf. dotted curve labeled "16" given in Figure 7a and solid curve labeled "Sys 1" in Figure 7c), supporting the notion of the importance of the short-range protein attraction to increase the probability of protein contacts in the adsorbed layer at low to intermediate adsorbed amount. Systems 2 and 3 display lateral rdf's similar to that of the reference system, but with a weak minimum at $\rho \approx 65$ Å.

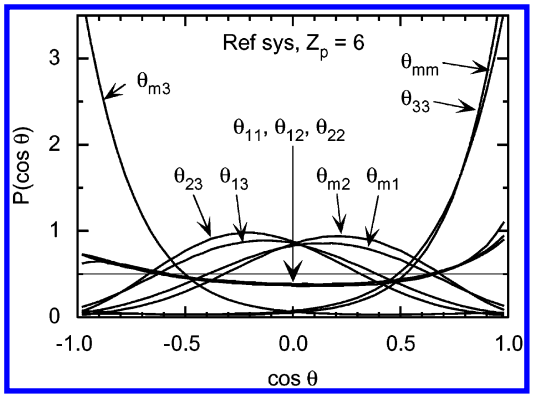

Figure 8. Normalized in-plane protein−protein orientational correlation functions $P(\cos\theta)$ of adsorbed proteins within 20 Å surface-to-surface separation for the reference system at the protein net charge $Z_p = 6$ and $\Gamma \approx 1.65$ mg/m^2 for indicated angles. The thin solid line at 0.5 denotes P for an isotropic orientation.

Thus, the lateral structure is strongly dependent on the adsorbed amount, but only weakly dependent on the protein net charge or other conditions, provided that the adsorbed amount is the same. The short-range protein−protein attraction makes the lateral structure considerably different from that of a two-dimensional hard-disk fluid. The discrepancy is largest at a small adsorbed amount and nearly vanishes at full surface coverage.

Protein−Protein Orientational Correlations. The relative orientation of neighboring proteins in the surface layer was also investigated by considering orientational correlation functions. From the simulations the probability of angles among $\mathbf{n}_m$ and $\mathbf{n}_\alpha$, $\alpha = 1, 2, 3$, was determined. More specifically, the 10 distinct correlation functions $P(\cos\theta_{\alpha\beta})$ $\alpha, \beta = m, 1, 2, 3$, for pairs of adsorbed proteins within 20 Å center-to-center separation were sampled.

The protein−protein orientational correlation functions for the reference system at $Z_p = 6$ and $\Gamma \approx 1.65$ mg/m^2 are shown in Figure 8. The functional forms of some of the correlation functions are similar, thus facilitating the analysis. To the first approximation, three sets can be distinguished. (A) The three correlation functions involving the angles θ_{mm}, θ_{m3}, and θ_{33} are all very similar (after considering the trivial change $\theta_{m3} \rightarrow \pi - \theta_{m3}$) with a high probability for $\cos\theta \approx 1$. Hence, any pair of the directions $\{\mathbf{n}_m, \mathbf{n}_3\}$ of neighboring proteins is to a large degree parallel. (B) Similarly, correlation functions involving the angles θ_{11}, θ_{12}, and θ_{22} are essentially equal and nearly constant, implying that correlations for any pair of the directions $\{\mathbf{n}_1, \mathbf{n}_2\}$ in neighboring proteins are small. (C) Finally, the remaining four correlation functions involving the angles θ_{m1}, θ_{m2}, θ_{13}, and θ_{23} formed by one of the directions $\{\mathbf{n}_m, \mathbf{n}_3\}$ and one of $\{\mathbf{n}_1, \mathbf{n}_2\}$ in neighboring proteins are all very similar (after considering $\theta_{13} \rightarrow \pi - \theta_{13}$ and $\theta_{23} \rightarrow \pi - \theta_{23}$), displaying a preferential perpendicular arrangement albeit the maximum of $P(\cos\theta)$ appearing slightly off $\cos\theta = 0$. As for the preferential orientation with respect to the surface normal, the protein−protein orientational correlation functions are essentially independent of the adsorbed amount (data not shown).

Now, since at $Z_p = 6$, $\mathbf{n}_m$ and $\mathbf{n}_3$ are nearly parallel, the following picture emerges. From (A), we conclude that the directions $\mathbf{n}_m$ and $\mathbf{n}_3$ of neighboring proteins are preferentially aligned, which is consistent with the analysis of $P(\cos \theta_{ms})$ and $P(\cos \theta_{3s})$. Observation (B) implies that the relative orientation *about* $\mathbf{n}_m$ and $\mathbf{n}_3$ of neighboring proteins are essentially uncorrelated; hence, there is no extensive energy barrier for rotation about $\mathbf{n}_m$ and $\mathbf{n}_3$. The absence of orientational correlation of θ_{11}, θ_{12}, and θ_{22} angles is consistent with the relative orientation of proteins with respect to the surface normal being unaffected by the adsorbed amount.

Hence, it seems that the protein−surface interaction controls the adsorbed amount and the protein orientation with respect to the surface normal, whereas the orientational-dependent protein−protein interaction is too weak to affect the adsorbed amount or to couple the orientation of neighboring proteins.

Discussion

In the following, some of our observations will be related to previous experimental and theoretical findings and some aspects of the model system and weaknesses of the model used addressed.

Comparison with Other Investigations. The adsorption of lysozyme onto mica[8,26,31,32,36] and other hydrophilic and negatively charged surfaces,[10,15,29,30,33−35,37,46−50] as well as the adsorption of other positively charged proteins on hydrophilic and negatively charged surfaces,[51−54] have been studied by a rich variety of techniques including ellipsometry,[46] total internal reflectance fluorescence (TIRF),[15] differential scanning calorimetry,[35] surface plasmon resonance spectroscopy,[50] surface force measurements,[8,32] ion exchange chromatography,[47−49] and neutron reflection.[10,33,34] Corresponding theoretical studies have also been carried out using different approaches.[13,16,55] These previous investigations on similar systems form a good base for comparison with the main findings of the present study.

Effect of Protein Net Charge on the Adsorbed Amount. The present study predicts an increased adsorbed amount at increasing protein net charge (experimentally obtained by decreasing pH) at constant surface charge density (Figure 3a). This is in agreement with findings from a previous simulation study by Oberholzer and Lenhoff,[55] using grand canonical Brownian dynamics for simulating adsorption isotherms for lysozyme adsorption onto a surface resembling negatively charged polystyrene sulfonate.

Experimentally, the situation is less clear and complicated by protein and surface titration frequently being difficult to practically separate. In several investigations, a bell-shaped pH dependence has been observed for lysozyme adsorption at hydrophilic surfaces, with a maximum near the isoelectric point of the lysozyme/sorbent complex.[27−29,31,52,56] Such a maximum adsorption at the isoelectric point has also been observed for other proteins.[54] Hence, at pH above the isoelectric point the adsorbed amount decreases, in agreement with the findings from our study (Figure 3a), whereas the experimental observed reduction of the adsorbed amount at decreasing pH below the isoelectric point is at variance with our predictions. On the other hand, increasing the charge contrast between the protein and the surface by changing the surface charge, which is predicted from our findings to result in an increased adsorption, has indeed been found also experimentally. Thus, Norde[54] investigated adsorption of RNase at hematite and found the adsorption to increase with pH above the isoelectric point of hematite. This suggests that the discrepancy between our present results on the effect of protein charge on the adsorption, on one hand, and those found experimentally, on the other, has its origin in the interprotein interaction, possibly its nonelectrostatic component. However, effects related to protein conformational changes, discussed frequently in relation to maximum adsorption at the isoelectric point,[54] cannot be ruled out.

Effect of Protein Ionic Strength on the Adsorbed Amount. Our study shows that the adsorption process is highly favored by low ionic strength (Figure 3b). In numerous studies, such a trend has been found for the adsorption of lysozyme[47−50] and other positively charged proteins[51−53] on hydrophilic and negatively charged surfaces. For example, Karst Lewus et al.[47] used gel-filled polystyrene-coated silica particles for ion-exchange chromatography to measure lysozyme adsorption and desorption. The equilibrium uptake was found to decrease gradually with ionic strength and no uptake occurred at salt concentrations of 0.3 M or greater. Also in our simulation no adsorption occurs with $I = 0.3$ M. Moreover, Oberholzer et al.[16,55] found in their simulation studies that the ionic strength had a strong effect on the adsorption, specifically that the adsorption decreased with an increasing ionic strength.

Structure of Adsorbed Layer. Our study shows that the adsorbed protein layer is composed essentially of a monolayer of proteins with scattered proteins forming a dilute second protein layer (Figure 4). Again, these findings are in agreement with experimental findings previously reported in the literature,[8,26,32−34,36] suggesting that lysozyme forms a dilute secondary layer when adsorbed to mica surfaces at high protein concentrations. As for the in-plane structure, comparison with experiments is precluded by the absence of detailed experimental results. It is noteworthy, however, that both Kim et al.[36] and Radmacher et al.[57] investigated lysozyme adsorption at mica with AFM and found indications of interfacial clustering of lysozyme. Within the model, such clustering before full surface coverage was inferred from the comparison of the lateral correlation function with the rdf for a hard-disk system (Figure 7a).

From the orientational analysis, our results indicate a strong preferential orientation of the proteins with respect to the surface normal, but essentially no other preferential orientational arrangement of the proteins. Direct experimental observations on the preferential orientation of adsorbed lysozyme are scarce. Nevertheless, earlier experimental studies[8,13] are discussed in terms of an orientation which places the positively charged residues of lysozyme close to the negatively charged surface, thereby maximizing the surface attraction. Furthermore, in a recent study by Daly et al.[37] the reorientation of lysozyme on silica surfaces was addressed by a combination of several techniques, and the results indicate a preferential orientation of adsorbed lysozyme, in agreement with our findings.

Role of Discrete Protein Charges. An interesting result of the present investigation is that electrostatic interactions may give rise to an adsorption of a net neutral protein to a charged surface, as well as adsorption even at conditions where the protein and the surface possess the same net charge. This was also found experimentally for lysozyme adsorbing at AgI [29] and negatively charged poly(styrenesulfonate)[28] particles, as lysozyme adsorbed also above the isoelectric point of lysozyme. Importantly, lysozyme adsorption was also found for lysozyme at mica at pH 12, corresponding to a protein net charge of -2.[31] Our results are also analogous to previous experimental results on protein−polyelectrolyte interactions, showing that the onset of complexation may occur at the same net sign of charge for the protein and the polyelectrolyte.[58,59] On the theoretical side, our results are in analogy with previously obtained findings by Ellis

et al.,[60] who performed simulations of the adsorption of a polyelectrolyte onto charged surfaces and found that adsorption could take place even if the sign of the net surface charge is the same as that of the polyelectrolyte.

Conclusions

Lysozyme adsorption to a negatively charged surface was studied by Monte Carlo simulations for a protein and a surface model containing discrete charges. The adsorption was favored by high protein concentration, high positive protein net charge, low ionic strength, and high negative surface charge density. Noticeably, adsorption of net negatively charged proteins on the negatively charged surface also appeared. Most of these findings are in qualitative agreement with experimental results. The lateral structure within the adsorbed layer becomes more ordered as the amount of protein at the surface increases. A tendency of a secondary layer formation of adsorbed proteins was found at large adsorbed amounts, again in agreement with experimental results. The adsorbed lysozyme molecules displayed a preferential orientation at the surface, which however is not sensitive on the adsorbed amount. While multipole expansion including monopole and dipole was not sufficient to explain preferential orientation, expansion including the quadropole provided a satisfactory picture. A strong preferential orientation may prevail even at weak adsorption. The attractive short-range protein−protein potential gave rise to an increased adsorbed amount at a given bulk concentration, and to an enhanced protein−protein contact in the adsorbed layer at a given adsorbed amount, but left the preferential orientation of adsorbed proteins unaffected.

The present model is naturally a gross simplification of adsorption of proteins from aqueous solutions to charged surfaces in general. Important shortcomings include: (i) the neglect of internal degrees of freedom, important in most cases of protein adsorption; (ii) the treatment of the solution as a medium by using a screened Coulomb potential; (iii) the description of the non-Coulomb attraction between lysozyme with a simple central potential; (iv) modeling of the shape of the protein as a hard sphere; and (v) omission of non-Coulomb attraction between proteins and the surface. Nevertheless, the model seems to capture many important features of lysozyme adsorption at hydrophilic and negatively charged surfaces, notably mica, observed also experimentally. Furthermore, it provides an initial step to describe how a discrete charge representation affects the orientation of adsorbed proteins and their ability to adsorb to surfaces with the same net charge.

Acknowledgment. Financial support from the Swedish Foundation for Strategic Research (SSF) through the graduate school Colloid and Interface Technology (CIT) is gratefully acknowledged.

References and Notes

(1) Mrksich, M.; Whitesides, G. M. *Ann. Rev. Biophys. Biomol. Struct.* **1996**, *25*, 55.
(2) Malmsten, M. *Biopolymers at Interfaces*; Marcel Dekker: New York, 2003; Vol. 110.
(3) Malmsten, M. *Surfactants and Polymers in Drug Delivery*; Marcel Dekker: New York, 2002.
(4) Rabel, S. R.; Stobaugh, J. F. *Pharm. Res.* **1993**, *10*, 171.
(5) Dickinson, E. *Food Hydrocolloids* **1986**, *1*, 3.
(6) Tolstoguzov, V. B. *Food Hydrocolloids* **1991**, *4*, 429.
(7) *Surface and Interfacial Aspects of Biomedical Polymers*; Andrade, J. D., Ed.; Plenum Press: New York, 1985; Vol. 2.
(8) Blomberg, E.; Claesson, P. M.; Fröberg, J. C.; Tilton, R. D. *Langmuir* **1994**, *10*, 2325.
(9) Haynes, C. A.; Norde, W. *J. Colloid Interface Sci.* **1995**, *169*, 313.
(10) Lu, J. R.; Thomas, R. K. The Application Of Neutron and X-ray Specular Reflection to Proteins at Interfaces. In *Physical Chemistry of Biological Interfaces*; Baszkin, A., Norde, W., Eds.; Marcel Dekker: New York, 2000; p 609.
(11) Adamczyk, Z.; Zembala, M.; Siwek, B.; Warszynski, P. *J. Colloid Interface Sci.* **1990**, *140*, 123.
(12) Yoon, B. J.; Lenhoff, A. M. *J. Phys. Chem.* **1992**, *96*, 3130.
(13) Roth, C. M.; Lenhoff, A. M. *Langmuir* **1993**, *9*, 962.
(14) Johnson, C. A.; Wu, P.; Lenhoff, A. M. *Langmuir* **1994**, *10*, 3705.
(15) Roth, C. M.; Lenhoff, A. M. *Langmuir* **1995**, *11*, 3500.
(16) Oberholzer, M. R.; Wagner, N. J.; Lenhoff, A. M. *J. Chem. Phys.* **1997**, *107*, 9157.
(17) Zhdanov, V. P.; Kasemo, B. *Surf. Rev. Lett.* **1998**, *5*, 615.
(18) Zhdanov, V. P.; Kasemo, B. *J. Chem. Phys.* **1998**, *109*, 6497.
(19) Wijmans, C. M.; Dickinson, E. *Phys. Chem. Chem. Phys.* **1999**, *1*, 2141.
(20) Wijmans, C. M.; Dickinson, E. *Langmuir* **1999**, *15*, 8344.
(21) Ravichandran, S.; Madura, J. D.; Talbot, J. *J. Phys. Chem. B* **2001**, *105*, 3610.
(22) Yu, K.; Li, Z.; Sun, J. *Langmuir* **2002**, *18*, 1419.
(23) Gekko, K.; Hasegawa, Y. *Biochemistry* **1986**, *25*, 6563.
(24) Norde, W.; Anusiem, A. C. I. *Colloids Surf.* **1992**, *66*, 73.
(25) Arai, T.; Norde, W. *Colloids Surf.* **1990**, *51*, 1.
(26) Tilton, R. D.; Blomberg, E.; Claesson, P. M. *Langmuir* **1993**, *9*, 2102.
(27) Haynes, C. A.; Sliwinsky, E.; Norde, W. *J. Colloid Interface Sci.* **1994**, *164*, 394.
(28) Galisteo, F.; Norde, W. *Colloids Surf. B* **1995**, *4*, 375.
(29) Galisteo, F.; Norde, W. *J. Colloid Interface Sci.* **1995**, *172*, 502.
(30) Buijs, J.; Hlady, V. *J. Colloid Interface Sci.* **1997**, *190*, 171.
(31) Koehler, J.; Ulbricht, M.; Belfort, G. *Langmuir* **1997**, *13*, 4162.
(32) Blomberg, E.; Claesson, P. M.; Fröberg, J. C. *Biomaterials* **1998**, *19*, 371.
(33) Su, T. J.; Lu, J. R.; Thomas, R. K.; Chui, Z. F.; Penfold, J. *Langmuir* **1998**, *14*, 438.
(34) Su, T. J.; Lu, J. R.; Thomas, R. K.; Chui, Z. F.; Penfold, J. *J. Colloid Interface Sci.* **1998**, *203*, 419.
(35) Larsericsdotter, H.; Oscarsson, S.; Buijs, J. *J. Colloid Interface Sci.* **2001**, *237*, 98.
(36) Kim, D. T.; Blanch, H. W.; Radke, C. J. *Langmuir* **2002**, *18*, 5841.
(37) Daly, S.; Przybycein, T. M.; Tilton, R. D. *Langmuir* **2003**, *19*, 3848.
(38) Carlsson, F.; Malmsten, M.; Linse, P. *J. Phys. Chem. B* **2001**, *105*, 9040.
(39) Carlsson, F.; Malmsten, M.; Linse, P. *J. Phys. Chem. B* **2001**, *105*, 12189.
(40) Carlsson, F.; Malmsten, M.; Linse, P. *J Am. Chem. Soc.* **2003**, *125*, 3140.
(41) Claesson, P. M. Thesis, Forces between Surfaces Immersed in Aqueous Solutions, The Royal Institute of Technology, 1986.
(42) Allen, M. P.; Tildesley, D. J. *Computer Simulation of Liquids*; Oxford University Press: Oxford, 1987.
(43) Linse, P. MOLSIM, version 3.3.5; Lund University, Sweden, 2002.
(44) Velev, O. D.; Kaler, E. W.; Lenhoff, A. M. *Biophys. J.* **1988**, *75*, 2682.
(45) Giarritta, S. P.; Ferrario, M.; Giaquinta, P. V. *Physica A* **1992**, *187*.
(46) Wahlgren, M.; Arnebrant, T.; Lundström, I. *J. Colloid Interface Sci.* **1995**, *175*, 506.
(47) Karst Lewus, R.; Altan, H. F.; Carta, G. *Ind. Eng. Chem. Res.* **1998**, *37*, 1079.
(48) Luo, Q.; Andrade, J. D.; Caldwell, K. D. *J. Chromatogr. A* **1998**, *816*, 97.
(49) Ghosh, R.; Cui, Z. F. *J. Liquid Chromatogr. Relat. Technol.* **2000**, *23*, 1619.
(50) Holmlin, E. R.; Chen, X.; Chapman, R. G.; Takayama, S.; Whitesides, G. M. *Langmuir* **2001**, *17*, 2841.
(51) Kondo, A.; Oku, S.; Higashitani, K. *J. Colloid Interface Sci.* **1991**, *143*, 214.
(52) Haynes, C. A.; Norde, W. *Colloids Surf. B: Biointerfaces* **1994**, *2*, 517.
(53) Zoungrana, T.; Findenegg, G. H.; Norde, W. *J. Colloid Interface Sci.* **1997**, *190*, 437.
(54) Norde, W. *Colloid Interface Sci.* **1986**, *25*, 267.
(55) Oberholzer, M. R.; Lenhoff, A. M. *Langmuir* **1999**, *15*, 3905.
(56) Johnson, J. E.; Matijevic, E. *Colloid Polym. Sci.* **1992**, *270*, 353.
(57) Radmacher, M.; Fritz, M.; Cleveland, J. P.; Walters, D. A.; Hansma, P. K. *Langmuir* **1994**, *10*, 3809.
(58) Xia, J.; Dubin, P. L.; Kim, Y.; Muhoberac, B. B.; Klimkowski, V. J. *J. Phys. Chem.* **1993**, *97*, 4528.
(59) Park, J. M.; Muhoberac, B. B.; Dubin, P. L.; Xia, J. *Macromolecules* **1992**, *25*, 290.
(60) Ellis, M.; Kong, C. Y.; Muthukumar, M. *J. Chem. Phys.* **2000**, *112*, 8723.